Physics of the Earth and Planetary Interiors 257 (2016) 12–17

Contents lists available at ScienceDirect

Physics of the Earth and Planetary Interiors

journal homepage: www.elsevier.com/locate/pepi

Ferrous iron partitioning in the lower mantle

Joshua M.R. Muir *, John P. Brodholt

Department of Earth Sciences, University College London, Gower Street, London WC1E 6BT, UK

ARTICLE INFO

Article history:
Received 18 June 2015
Received in revised form 4 April 2016
Accepted 12 May 2016
Available online 21 May 2016

Keywords:
Ferropericlase
Bridgmanite
Partitioning
Lower mantle

ABSTRACT

We used density functional theory (DFT) to examine the partitioning of ferrous iron between periclase and bridgmanite under lower mantle conditions. To study the effects of the three major variables — pressure, temperature and concentration — these have been varied from 0 to 150 GPa, from 1000 to 4000 K and from 0 to 100% total iron content. We find that increasing temperature increases K_D, increasing iron concentration decreases K_D, while pressure can both increase and decrease K_D. We find that K_D decreases slowly from about 0.32 to 0.06 with depth under lower mantle conditions. We also find that K_D increases sharply to 0.15 in the very lowermost mantle due to the strong temperature increases near the CMB. Spin transitions have a large effect on the activity of ferropericlase which causes K_D to vary with pressure in a peak-like fashion. Despite the apparently large changes in K_D through the mantle, this actually results in relatively small changes in total iron content in the two phases, with X_{Fe}^{fp} ranging from about 0.20 to 0.35, before decreasing again to about 0.28 at the CMB, and X_{Fe}^{bd} has a pretty constant value of about 0.04–0.07 throughout the lower mantle. For the very high Fe concentrations suggested for ULVZs, Fe partitions very strongly into ferropericlase.

1. Introduction

The presence of iron and its oxidation state has a major effect on the structure and dynamics of minerals in the Earth's interior. For instance, the concentration of iron affects the density, elasticity, electrical conductivity, melting temperature and melt compositions, diffusion rates and the rheological properties of the host mineral. Iron concentrations also affect the sharpness of phase transitions (see for example pv to ppv (Catalli et al., 2009)), and the onset and width of spin transitions. In addition, spin transitions in ferropericlase have been suggested to cause strong depletions of Fe in bridgmanite and strong enrichments in ferropericlase (e.g. (Auzende et al., 2008; Badro et al., 2003; Holmstrom and Stixrude, 2015; Lin et al., 2005; Vilella et al., 2015)). This in turn changes the physical properties of the mantle in those areas (see for example Lin et al. (2013)).

The lower mantle is over 90% bridgmanite (bd) and ferropericlase (fp) with typical iron concentrations of around 10% by weight. Although the partitioning of iron between these phases at pressures ~20–110 GPa and at ~2000–2600 K has been studied experimentally and with thermodynamic modelling a number of times (Auzende et al., 2008; Guyot et al., 1988; Katsura and Ito, 1996; Mao et al., 1997; Nakajima et al., 2012; Narygina et al., 2011; Sakai et al., 2009; Sinmyo et al., 2008), there are still discrepancies between different studies. The partitioning reaction is defined as:

$$MgSiO_3^{bd} + FeO^{fp} \leftrightarrow FeSiO_3^{bd} + MgO^{fp} \quad \text{(Reaction1)}$$

and the partition coefficient K_D is defined at equilibrium as:

$$K_D = \frac{\frac{X_{FeSiO_3}^{bd}}{X_{MgSiO_3}^{bd}}}{\frac{X_{FeO}^{fp}}{X_{MgO}^{fp}}} \quad (1)$$

where X_i^a is the mole fraction ratio of component i in phase a. All studies show that iron prefers fp to bd but there are some differences as to what degree fp is favoured. For instance, at 100 GPa and about 2000 K, K_D varies between about 0.07 and 0.25 depending on the particular study in Mg_2SiO_4 mixtures (Auzende et al., 2008; Nakajima et al., 2012; Narygina et al., 2011; Sakai et al., 2009; Sinmyo et al., 2008; Tange et al., 2009). There are also small differences on the effect of pressure on K_D; pressure tends to decrease K_D at a rate of around 0.001–0.002 K_D/GPa, but this again depends upon the particular study. Most studies only have a small temperature range but thermodynamic modelling shows that increasing temperature tends to increase K_D on the order of ~0.1 K_D for every 1000 K (Nakajima et al., 2012). Increasing the overall iron concentration has the effect of reducing K_D (Nakajima et al., 2012), although individual studies tend to have small ranges in

* Corresponding author.
E-mail address: joshua.muir@ucl.ac.uk (J.M.R. Muir).

http://dx.doi.org/10.1016/j.pepi.2016.05.008
0031-9201/

concentration and so the magnitude of this effect is subject to some uncertainty when extrapolated away from the experimental compositions.

As well as the somewhat inconsistent results from different experimental studies and the limited range of compositions and temperature in experiments which makes extrapolation difficult, additional complications arise with more realistic systems. For instance, ferric iron does not affect ferrous iron partitioning when it is monitored and removed from calculations of iron content (Frost and Langenhorst, 2002; Kesson et al., 2002; Mao et al., 1997; McCammon et al., 2004), but the concentration of ferric iron can be affected by total iron concentration, oxygen fugacity, aluminium content and ferric and ferrous spin transitions and thus can drastically vary K_D (Fujino et al., 2014; Nakajima et al., 2012; Prescher et al., 2014; Sinmyo and Hirose, 2013). In addition, spin transitions in both bd and fp are known to affect iron partitioning (Auzende et al., 2008; Fujino et al., 2014; Irifune et al., 2010; Nakajima et al., 2012; Prescher et al., 2014; Sakai et al., 2009; Sinmyo and Hirose, 2013) and so the spin state needs to be known when extrapolating to different conditions. Pyrolitic compositions, as opposed to Mg_2SiO_4 compositions, tend to have larger K_D values of around ~0.4–1 (Fujino et al., 2014; Irifune et al., 2010; Prescher et al., 2014; Sinmyo and Hirose, 2013).

In this work we use DFT methods to calculate the partitioning of Fe^{2+} between ferro-periclase and bridgmanite. This method has the benefit of being free from the issues of ferric iron contamination, and spin states can be explicitly known and varied. We can also examine the effect of large concentrations of iron on K_D, which are potentially important in some regions of the mantle (Bower et al., 2011; Dobson and Brodholt, 2005; Mao et al., 2006; Muir and Brodholt, 2015a; Wicks et al., 2010). Moreover, we can also study higher pressures and temperature than have been achieved experimentally before (up to 150 GPa and 4000 K).

2. Methods

2.1. Theoretical details

All simulations were carried out with the DFT code VASP (Kresse and Furthmuller, 1996) using the projector-augmented-wave (PAW) method (Kresse and Joubert, 1999) and the PBE formulation of GGA corrected for solids (Perdew et al., 2008). The core radii of the PAW spheres are O 0.80 Å ($2s^2 2p^4$), Si 1.00 Å ($3s^2 3p^2$), Mg 1.06 Å ($2p^6 3s^2$), Fe 1.22 Å ($3d^7 4s^1$). 14 electron Fe potentials were also tested and the results are similar. To account for GGA's inability to correctly reproduce iron spin states we used a GGA+U functional with Hubbard U parameters set to 3 eV. This value has been estimated for fp from optical spectroscopy (Goncharov et al., 2006) and has been used theoretically to produce spin crossovers similar to experiments (Persson et al., 2006). A slightly smaller value (2.5 eV) has also been used to replicate experimental results (Holmstrom and Stixrude, 2015). Similarly this same value has been used to replicate experimental spin crossovers in bd (Huang and Pan, 2012).

For ferropericlase we used a cubic 64 atom unit cell (2a*2a*2a) and for bridgmanite an 80 unit cell (2a*2b*c). To calculate the variation in free energy of reaction 1, both enthalpies and entropies have to be determined.

Enthalpies were determined statically (i.e. at 0 K) with an energy cutoff of 850 eV, 6 × 6 × 6 k points and self-consistent runs that were relaxed to within 10^{-6} eV.

Molecular dynamics (MD) simulations were run to obtain properties at high T using an NVT ensemble with the Nosé thermostat (Nose, 1984) and with Nosé frequencies of ~20 THz. MD calculations were run at the gamma point with a cutoff of 500 eV, relaxation to within 10^{-4} eV and were run for 10 ps. The electronic entropy was determined directly from VASP. Magnetic entropy was determined using Eq. (2):

$$S_{mag} = \ln(\mu + 1) \times R \times n_{Fe} \quad (2)$$

where R is the gas constant and μ is the average absolute magnetic moment of an individual iron atom determined from VASP. Note that this does not contain a term for magnetic degeneracy since that is already contained in the electronic entropy. It is assumed that iron states are fully paramagnetic.

To determine vibrational entropy contribution to fp and bd we used thermodynamic integration with the blue-moon algorithm in VASP (Bucko, 2008). This calculates the difference between two states (here different temperatures) by calculating the free-energy gradient along a constrained reaction path. This is done by calculating the restoring force between the constrained and unconstrained reaction path. The restoring force is then integrated to give a free energy difference between the initial and final state. The reaction path constraints were placed on the Fe–O and Fe–Fe bond lengths in iron-bearing systems and Mg–O and Mg–Mg in iron-free systems, as these lengthen upon heating. However, the choice of reaction path is irrelevant when calculating the free energy between 2 final states as the free energy is a state function. At each temperature, pressure and composition (i.e. concentration of Fe) investigated, the free energy was calculated between a system (fp or bd) at 0 K and the same system at the temperature of interest using 6 image paths (different temperatures) and the path energies were integrated to give a vibrational free energy difference (ΔG) between the 0 K and the heated system. This is fundamentally identical to calculating the variation of heat capacity divided by temperature between fp and bd systems.

2.2. Calculating K_D

The enthalpy and entropy were determined for $Fe_xMg_{1-x}O$ and $Fe_xMg_{1-x}SiO_3$ with x = 0, 0.25, 0.5, 0.75 and 1 at 30, 60, 90, 130 and 150 GPa and at 1000, 2000 and 4000 K. Fp calculations involve a mixed spin state and the method of calculating the free energy of this state is outlined in Muir and Brodholt, 2015a. As calculating the free energy of every possible arrangement of iron in each concentration would be computationally onerous, all calculated arrangements had iron at the maximum separation from each other and it is assumed that the possible formation of iron clusters does not overly affect the partitioning (atom positions at 0 GPa are included in File S1 and S2).

Once enthalpy and entropies of fp and bd systems were obtained the K_D of Reaction 1 was calculated with Eq. (3):

$$RT \ln K_D = -\Delta G^0_{P,T} - RT \ln \frac{\gamma^{bd}_{Fe}/\gamma^{bd}_{Mg}}{\gamma^{fp}_{Fe}/\gamma^{fp}_{Mg}} \quad (3)$$

where R is the gas constant, T is temperature, $-\Delta G^0_{P,T}$ is the standard state Gibbs free energy change between the end members at the pressure, temperature and composition of interest and includes magnetic, vibrational and electronic entropy, and γ^a_i is the activity coefficient of Fe or Mg in either phase and accounts for the non-ideality of Fe–Mg mixing in each solid solution.

To calculate the activity coefficients we first calculated a set of Margules parameters (Walas, 1985) using the equation:

$$\frac{G_{mix}}{RT} = X_{Fe}X_{Mg}\left(X_{Mg}W_{Fe-Mg} + X_{Fe}W_{Mg-Fe}\right) \quad (4)$$

where Gmix is the difference in energy between a linear mixture of FeO and MgO (or $FeSiO_3$ and $MgSiO_3$) and the calculated energy of $Fe_xMg_{1-x}O$ (or $Fe_xMg_{1-x}SiO_3$). For each phase (bd or fp) this was solved simultaneously for x = 0.25, x = 0.5 and x = 0.75 to get both

parameters (W_{Fe-Mg} and W_{Mg-Fe}). Activity coefficients are then calculated using Eq. (5):

$$RT \ln \gamma_{Fe}^{bd} = \left(X_{MgSiO_3}^{bd}\right)^2 \left[W_{Fe-Mg}^{bd} + 2X_{FeSiO_3}^{bd}\left(W_{Mg-Fe}^{bd} - W_{Mg-Fe}^{bd}\right)\right] \quad (5)$$

where appropriate substitutions can be made to determine all 4 activity coefficients.

Eq. (3) was then solved with the assumption that the total amount of iron in the system is conserved.

3. Results

The partitioning of iron between fp and bd depends upon the enthalpy of formation, entropy variations and non-ideal mixing factors. These factors, however, all depend upon the spin-state of the ferrous iron which can either be high spin ($S = 2$) or low spin ($S = 0$) in both fp and bd. Thus the spin states of iron in the various systems must first be calculated.

3.1. Spin states

As outlined in Muir and Brodholt (2015b) we find ferrous iron in bridgmanite to be high spin for all mantle pressures/temperatures and for all iron concentrations. We shall therefore, treat ferrous iron in bridgmanite as high spin.

Ferrous iron in fp is more problematic due to the well-documented presence of mixed-spin states at mantle conditions (Lin et al., 2013). As outlined and using the method in Muir and Brodholt (2015a), we predict the presence of a mixed spin state which contains both high and low spin iron for all iron concentrations at lower mantle pressures and temperatures. Fig. 1 shows some of the ratios of high spin to low spin in fp against the three controlling variables- temperature, pressure and total iron concentration. Increasing temperature or iron concentration increases the amount of high spin iron, whereas increasing pressure increases the amount of low spin iron in fp. The $-\Delta S/\Delta V$ value is 0.016 in GPa/K which is similar to the values of 0.015–0.017 found in Fukui et al. (2012), Wentzcovitch et al. (2009), Wu et al. (2009) and slightly lower than the value of 0.012 in Holmstrom and Stixrude (2015); the slightly smaller value makes sense as Holmstrom and Stixrude (2015) included an additional term for nonideal mixing between high and low spin iron.

3.2. Enthalpy

The enthalpy and volume change of reaction 1 is shown in Fig. 2. The enthalpy change depends upon the spin state of Fe in the ferropericlase phase. With Fe in fp fixed in the low spin state, enthalpy acts to favour iron in the bd phase below 25 GPa and in the fp phase above 25 GPa. When Fe spin in fp is fixed in the high spin state or when the spin is allowed to find its own state (spins being a mixture of high and low spin), enthalpy favours iron in the fp phase at all pressures. With increasing pressure, iron increasingly prefers the fp phase as the reactants of reaction 1 are denser than the products of reaction 1. We find a consistent increase in the density change of reaction 1 with pressure, unlike the values predicted in Nakajima et al. (2012) where the volume change of the reaction was independent of pressure.

The enthalpy values in Fig. 2 are for the iron end members ($x = 1$ in $Fe_xMg_{2-x}SiO_4$). With decreasing iron concentration ($x = 0.25$ and $x = 0.5$) there is a roughly linear decrease in ΔH. This acts to decrease K_D with increasing iron concentration. Lowering the Fe concentration also stabilises the low spin state in fp, which will slightly affect the shape of the K_D curve (see below).

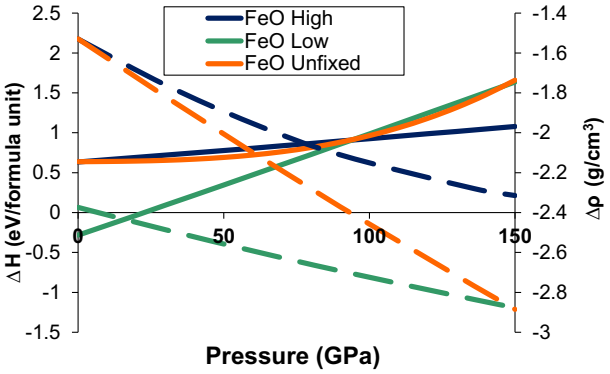

Fig. 2. Enthalpy (ΔH) (solid lines, left vertical axis) (with positive values favouring Fe in fp) and density changes ($\Delta\rho$) (with negative values favouring Fe in fp) (dashed lines, right axis) of reaction 1 ($x = 1$, $FeMgSiO_4$) at static conditions. The unfixed spin state is a system with no spin fixing at 0 K and has a mixture of high and low spin depending upon the pressure. Thermal entropy effects are not shown as they are very small (<0.07 meV/K at 0 GPa and decreasing with pressure).

3.3. Entropy

The entropy contributions to reaction 1 as a function of pressure are shown in Fig. 3. Electronic entropy varies slightly between fp and bd, but has a negligible effect on the overall K_D and is not shown in Fig. 3. The magnetic entropy is 0 for low spin ferrous iron

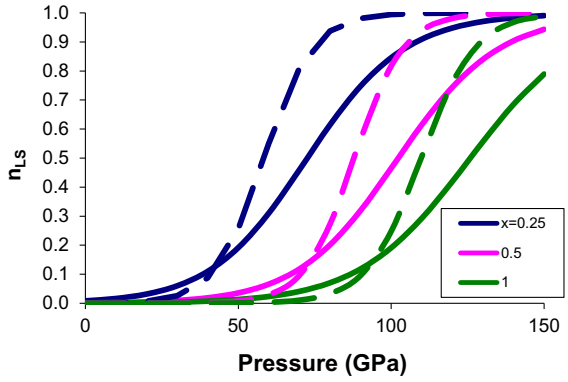

Fig. 1. Proportion of low spin sites for $Fe_xMg_{1-x}O$ at 2000 K (solid lines) and 1000 K (dashed lines) with varying pressure.

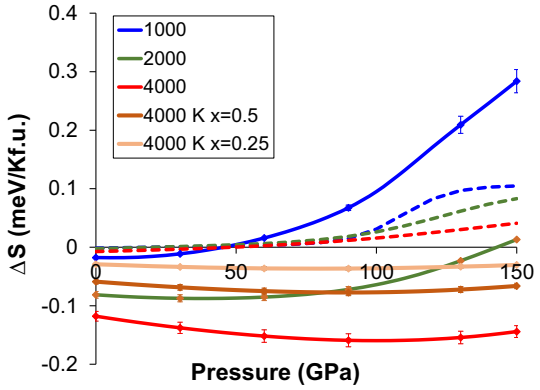

Fig. 3. Entropy (ΔS) of reaction 1 (with $Fe_xMg_{2-x}SiO_4$), with positive values favouring partitioning of Fe into bridgmanite. Solid lines are vibrational entropy and dashed lines are magnetic entropy. Electronic entropy differences are negligible. For $x < 1$ only the vibrational entropy at 4000 K is shown, the entropy of these systems decreased in a roughly linear fashion for all cases. Error is the statistical error of molecular dynamics and is mostly the error in calculated temperature.

and Mg and ~0.1 meV/f.u. for high spin ferrous iron. Magnetic entropy differences between FeO and $FeSiO_3$ are therefore only significant when FeO is mostly low spin. This can be seen at the high pressure end of Fig. 3 where the magnetic entropy difference of the reaction approaches a maximum of ~0.1 meV/f.u. With lower concentrations of iron this maximum is reached at a lower pressure due to the decreased spin transition pressure, but the maximum entropy difference also decreases in a linear fashion depending upon the amount of iron present.

Both of these factors, however, are much smaller than the differences in the vibrational entropy. Vibrational entropy differences have a complicated relationship between pressure, spin state and temperature. At 1000 K, vibrational entropy acts to stabilise the products of reaction 1 above 50 GPa. This behaviour, however, changes strongly with temperature and above 2000 K, vibrational ΔS switches sign. The differences in vibrational entropy are strongly amplified by pressure.

Decreasing the iron concentration decreases the magnitude of vibrational entropy linearly. Slight changes to the vibrational entropy of FeO due to varying high and low spin ratios in FeO are minimal compared to vibrational entropy differences between FeO and MgO and $FeSiO_3$–bd.

While the calculation of entropy differences is more accurate than the calculation of absolute entropies — due to cancellation of errors from choice of exchange–correlation functional for instance — it is still worth comparing our entropies with those available in the literature. These are shown in Fig. 4 for bridgmanite (Metsue and Tsuchiya, 2012) and MgO (Scanavino et al., 2012). The literature values are obtained via lattice dynamics, while ours use MD and thermodynamic integration as described above. Nevertheless, there is a satisfying agreement and as can be seen, the entropies agree within statistical error. Differences between our results and those of the literature increase as temperature increases. This is to be expected as anharmonic effects which are not included in lattice dynamics techniques will increase with temperature.

3.4. Non-ideality

Fig. 5 (and Table S1) shows the calculated Margules parameters for bd and fp. As can be seen, the fp Margules parameter increase considerably with pressure, something that is not captured in previous low pressure (25 GPa) results (Fei et al., 1991; Frost, 2003). Above about 50 GPa the non-ideality in the mixing of Mg and Fe in fp becomes increasingly important due to the spin states of fp.

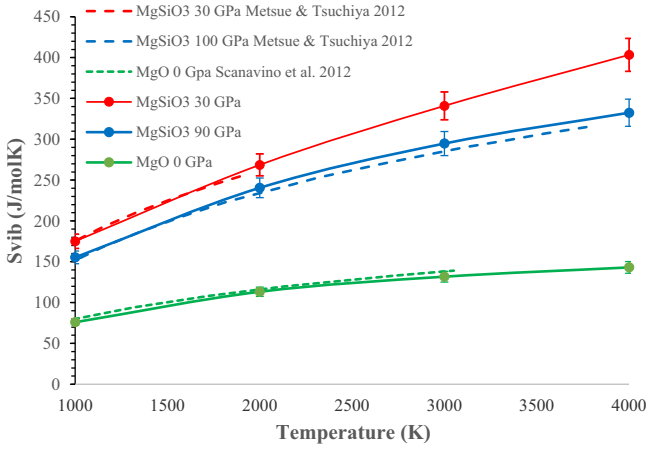

Fig. 4. Comparison of the absolute vibrational entropy of our iron-free products with data in Metsue and Tsuchiya (2012) and Scanavino et al. (2012). These both use lattice dynamics methods.

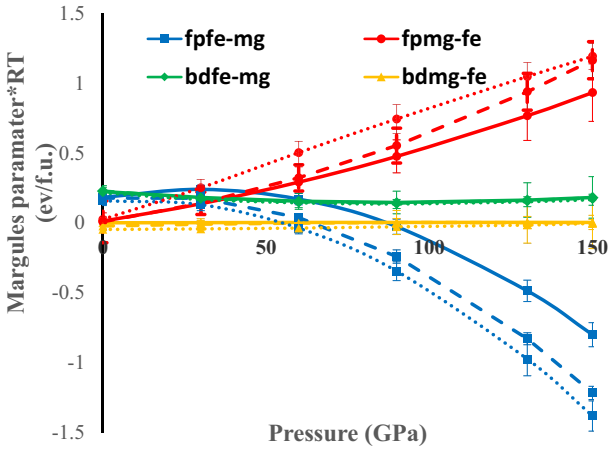

Fig. 5. Margules parameters for $Fe_xMg_{1-x}O$ and $Fe_xMg_{1-x}SiO_3$ calculated with $x = 0.25$, 0.5 and 0.75 and at 1000 K (dotted lines), 2000 K (dashed lines) and 4000 K (solid lines). For bridgmanite there is little deviation in Margules parameters with temperature compared to ferropericlase. Error bars are calculated from the statistical error in G and are mostly due to uncertainty in temperature. Errors in Mg parameters are larger than those in Fe parameters due to the greater uncertainty in $x = 0.75$ compared to $x = 0.25$ structures.

The large effect of the spin transition also prevents the use of symmetric Margules parameters above around 25 GPa, in response to the temperature dependence of the spin transition. There is no spin transition in bd and so the Margules parameters for bd are much smaller than those of fp and have a much less important role in determining K_D.

3.5. Partitioning

Fig. 6 shows our calculated K_D for $Mg_{2-x}Fe_xSiO_4$ mixtures with $x = 0.25$, 0.5 and 1 against pressure at temperatures of 1000, 2000 and 4000 K. The values are also given in Table S2. Pressure, temperature and iron concentration all have an effect on K_D.

K_D for typical iron concentrations ($x = 0.25$ and 0.5) initially increases and then decreases with pressure. This effect is mostly driven by the spin transition in fp. Before the spin transition K_D

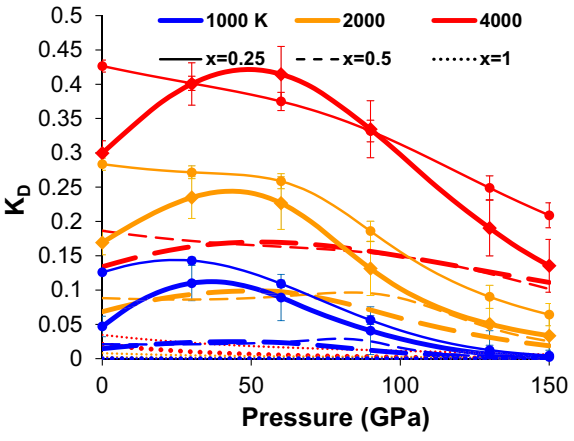

Fig. 6. K_D for bd/fp mixtures ($Mg_{2-x}Fe_xSiO_4$) where $x = 0.25$ (solid lines), $x = 0.5$ (dashed lines) and $x = 1$ (dotted lines) at various temperatures as a function of pressure. Thick lines are the calculated K_D with the Margules parameters in Fig. 5, thin lines are a fictitious K_D where all Margules parameters have been set to 0. For $x = 0.25$ calculated points have been plotted including errors- these errors bars represent the statistical error in entropy and temperature for both G and Margules parameters but do not include inherent errors in DFT energy. For clarity points for $x = 0.5$ and $x = 1$ have been plotted but were at the same pressures as for $x = 0.25$ and have similar errors.

is driven upwards by pressure due to activity effects, after the spin transition K_D is driven downwards due to the combined effect of activity and the energy/volume change of the reaction. In other words, without the spin transition K_D would increase until Fe is partitioned equally between bridgmanite and ferropericlase. The fact that pressure and spin act in an opposite way means that K_D does not change much through the mantle (see Fig. 6), except in the lowermost mantle where very low values of K_D are found. Similar behaviour has been seen for pyrolitic compositions (Irifune et al., 2010) and possibly for pv/bd mixtures (Auzende et al., 2008). For high iron concentrations ($x = 0.75$) the activity behaviour is reversed and so K_D peaks show the opposite behaviour (initially decreasing and then increasing with pressure), though the peaks are much shallower in these cases as activity becomes less important compared to enthalpy with increasing iron concentration.

Increasing the temperature increases K_D for all compositions and pressures. This is as expected and is caused by the vibrational entropy effects outlined above, together with the entropy of mixing driving Fe into both phases. A final temperature effect is that of temperature on the spin states of fp.

The total amount of iron in the system also affects K_D, with K_D increasing with decreasing amounts of total iron. The peak in K_D also moves with iron concentration, depending on how the spin transition changes with concentration.

To demonstrate the effect of non-ideality on K_D, Fig. 6 also shows calculations with the Margules parameters set to 0. As can be seen the general trend is similar, and the effect of non-ideality is to vary the shape of the K_D vs pressure.

Fig. 7 shows our calculated K_D at 2000 K for a $x = 0.25$ fp/bd mixture against various literature values. Our results are within the range of experimental values, although there is considerable spread in the experimental data. The data of Sakai et al. (2009) and Auzende et al. (2008) have a similar K_D/pressure slope to ours, with the data of Narygina et al. (2011) and Nakajima et al. (2012) having less pronounced slopes. The data of Tange et al. (2009) presents a much steeper K_D slope with pressure which is quite different to our data and starts considerably before any expected spin transition. It's not clear what causes the large variation in partitioning of iron between bd and fp obtained experimentally. It has been shown that when starting from olivine, equilibrium partitioning occurs in under 10 min (Martinez et al., 1997) so these differences are unlikely to be related to diffusion. On the other hand, it has been shown in Sinmyo et al. (2008) that small scale heterogeneities in olivine can cause large errors in K_D on a scale similar to the experimental spread.

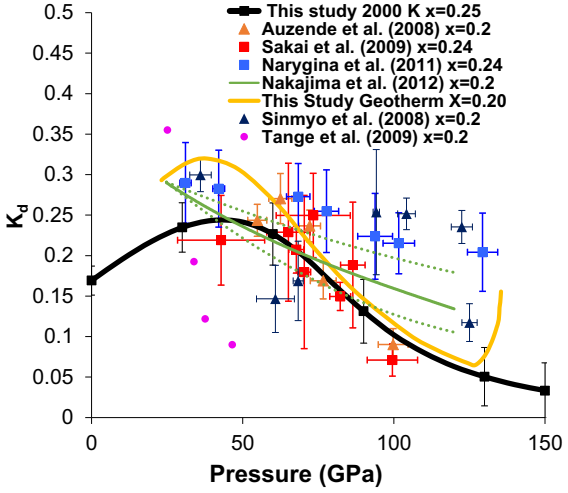

Fig. 7. Plot showing our calculated K_D compared with experimental values from the literature. Measurements were performed between 2000–2400 K for Auzende et al. (2008), 1860–2120 K for Sakai et al. (2009), 1760–2130 K for Sinmyo et al. (2008), 1500 K for Tange et al. (2009) and at 1950 K for Narygina et al. (2011). The green line is from Nakajima et al. (2012) constructed using a thermodynamic model constrained by multi-anvil measurements. This line is constructed at 2000 K and the dotted green lines are the uncertainties. Our calculated values are in black, with errors as stated in Fig. 6. Additionally the orange line is K_D of an $x = 0.2$ bd/fp mixture along a lower mantle geotherm (Ono, 2008) up to the core-mantle boundary at 2890 km. (For interpretation of the references to colour in this figure legend, the reader is referred to the web version of this article.)

Table 1
Molar ratio of Fe (Fe/Fe + Mg) in fp and bd phases along a lower mantle geotherm (Ono, 2008) with $x = 0.20$ and with a bd:fp ratio of 80:20. Error values are from the statistical errors in MD simulations. The values from Narygina et al. (2011) were calculated using the (three interval) K_D data along a geotherm that is presented in that paper and then applying the two conditions above.

Depth (km)	This work		Narygina et al. (2011)	
	X_{Fe}^{fp}	X_{Fe}^{bd}	X_{Fe}^{fp}	X_{Fe}^{bd}
650	0.210 ± 0.009	0.072 ± 0.003		
850	0.203 ± 0.011	0.074 ± 0.003	0.211	0.072
1250	0.207 ± 0.012	0.073 ± 0.003	0.208	0.073
1500	0.222 ± 0.014	0.069 ± 0.004	0.208	0.073
1750	0.246 ± 0.021	0.063 ± 0.005	0.214	0.072
2000	0.272 ± 0.021	0.057 ± 0.006	0.217	0.071
2500	0.276 ± 0.022	0.056 ± 0.007	0.214	0.071
2790	0348 ± 0.023	0.038 ± 0.011		
2890	0.276 ± 0.023	0.056 ± 0.007		

Also shown in Fig. 7 is K_D along a mantle geotherm for a $Mg_{2-x}Fe_xSiO_4$ fp/bd mixture with $x = 0.2$ (10% iron concentration). Throughout most of the lower mantle K_D decreases with depth from 0.32 to 0.06. From 2550–2890 km, where the geotherm includes a sharp temperature rise to ~4000 K, there is a corresponding sharp rise in K_D to about 0.15 at the CMB.

The concentrations of Fe in fp and bd steadily increase and decrease respectively throughout the lower mantle (Table 1), with X_{Fe}^{fp} ranging from about 0.20 to 0.35, before decreasing again to about 0.28 at the CMB. Similarly, X_{Fe}^{bd} has a pretty constant value of about 0.04–0.07 throughout the lower mantle. The composition of bridgmanite and ferropericlase in the lower mantle should, therefore, be relatively homogenous with only small changes in iron concentrations in the two phases.

At very high concentrations (~100%) of iron, K_D should be below 0.01 under all conditions, and almost all iron partitions into fp. These results support highly-iron enriched ULVZs suggested in Muir and Brodholt (2015a), which required strong iron partitioning into fp.

4. Conclusions

We have examined the partitioning of ferrous iron between ferropericlase and bridgmanite for all mantle pressures and temperatures, and over a large range in total iron content. In agreement with all experimental data, we find that ferrous iron prefers ferropericlase to bridgmanite. We find that spin transitions have a large effect on the response of K_D to pressure. For typical iron concentrations in the mantle, K_D increases up to about 0.32 at about 30–50 GPa where spin transitions cause it to decrease to 0.06 at 120 GPa. K_D then increases in D″ to about 0.15 at the CMB. Despite the apparently large changes in K_D through the mantle, this actually results in relatively small changes in total iron content in the two phases, with X_{Fe}^{fp} ranging from about 0.20 to 0.35, before decreasing again to about 0.28 at the CMB, and X_{Fe}^{bd} has a pretty constant value of about 0.04–0.07 throughout the lower mantle.

At very high concentrations of Fe, the partitioning of iron strongly favours ferropericlase. This strong enrichment of Fe in ferropericlase is required for Fe-enrichment to be the cause of ULVZs.

This study concentrates on Fe^{2+} only and ignores the role Fe^{3+} and its association with Al^{3+}. Although the exact nature of spin transitions in Fe^{3+} in bridgmanite are still not totally resolved, recent studies suggest that this spin transition could also affect the partitioning of ferric iron between ferropericlase and bridgmanite (Fujino et al., 2014; Prescher et al., 2014; Sinmyo and Hirose, 2013). We have yet to calculate the portioning of ferric iron between these phases and this remains a fruitful line of further research.

Acknowledgements

The research in this proposal was supported by NERC Grants NE/H021027/1 and NE/M00046X/1. Calculations were run on the UK National HPC facility, ARCHER. The authors would like to thank the many helpful reviewers that suggested improvements to this work.

Appendix A. Supplementary data

Supplementary data associated with this article can be found, in the online version, at http://dx.doi.org/10.1016/j.pepi.2016.05.008.

References

Auzende, A.-L., Badro, J., Ryerson, F.J., Weber, P., Fallon, S., Addad, A., Siebert, J., Fiquet, G., 2008. Element partitioning between magnesium silicate perovskite and ferropericlase: new insights into bulk lower-mantle geochemistry. Earth Planet. Sci. Lett. 269, 164–174.

Badro, J., Fiquet, G., Guyot, F., Rueff, J., Struzhkin, V.V., Vanko, G., Monaco, G., 2003. Iron partitioning in earth's mantle: toward a deep lower mantle discontinuity. Science 300, 789–791.

Bower, D.J., Wicks, J.K., Gurnis, M., Jackson, J.M., 2011. A geodynamic and mineral physics model of a solid-state ultralow-velocity zone. Earth Planet. Sci. Lett. 303, 193–202.

Bucko, T., 2008. Ab-initio calculations of free-energy reaction barriers. J. Phys. Condens. Mater. 20, 1–9.

Catalli, K., Shim, S.-H., Prakapenka, V., 2009. Thickness and Clapeyron slope of the post-perovskite boundary. Nature 462, 782–785.

Dobson, D.P., Brodholt, J.P., 2005. Subducted banded iron formations as a source of ultralow-velocity zones at the core-mantle boundary. Nature 434, 371–374.

Fei, Y., Mao, H.-K., Mysen, B., 1991. Experimental determination of element partitioning and calculation of phase relations in the MgO–FeO–SiO_2 system at high pressure and high temperature. J. Geophys. Res. 96, 2157–2169.

Frost, D.J., 2003. Fe^{2+}–Mg partitioning between garnet, magnesiowüstite, and (Mg, Fe)$_2SiO_4$ phases of the transition zone. Am. Mineral. 88, 387–397.

Frost, D.J., Langenhorst, F., 2002. The effect of Al_2O_3 on Fe–Mg partitioning between magnesiowustite and magnesium silicate perovskite. Earth Planet. Sci. Lett. 199, 227–241.

Fujino, K., Nishio-Hamane, D., Nagai, T., Seto, Y., Kuwayama, Y., Whitaker, M.L., Ohfuji, H., Shinmei, T., Irifune, T., 2014. Spin transition, substitution, and partitioning of iron in lower mantle minerals. Phys. Earth Planet. Inter. 228, 186–191.

Fukui, H., Tsuchiya, T., Baron, A., 2012. Lattice dynamics calculations for ferropericlase with internally consistent LDA+U method. J. Geophys. Res. 117, B122021-10.

Goncharov, A.F., Struzhkin, V.V., Jacobsen, S.D., 2006. Reduced radiative conductivity of low-spin (Mg, Fe)O in the lower mantle. Science 312, 1205–1208.

Guyot, F., Madon, M., Peyronneau, J., Poirier, J.P., 1988. X-ray microanalysis of high-pressure/high-temperature phases synthesized from natural olivine in a diamond-anvil cell. Earth Planet. Sci. Lett. 90, 52–64.

Holmstrom, E., Stixrude, L., 2015. Spin crossover in ferropericlase from first-principles molecular dynamics. Phys. Rev. Lett. 114, 1172021–1172025.

Huang, D., Pan, Y., 2012. Pressure-induced spin transitions of iron in $MgSiO_3$ perovskite: a GGA+U study. High Pressure Res. 32, 270–279.

Irifune, T., Shinmei, T., McCammon, C., Miyajima, N., Rubie, D.C., Frost, D.J., 2010. Iron partitioning and density changes of pyrolite in Earth's lower mantle. Science 327, 193–195.

Katsura, T., Ito, E., 1996. Determination of Fe–Mg partitioning between perovskite and magnesiowiistite. Geophys. Res. Lett. 23, 2005–2008.

Kesson, S.E., Fitz Gerald, J.D., O'Neill, H.S.C., Shelley, J.M.G., 2002. Partitioning of iron between magnesian silicate perovskite and magnesiowüstite at about 1 Mbar. Phys. Earth Planet. Inter. 131, 295–310.

Kresse, G., Furthmuller, J., 1996. Efficient iterative schemes for ab-initio total-energy calculations using a plane-wave basis set. Phys. Rev. B 54, 11169–11186.

Kresse, G., Joubert, D., 1999. From ultrasoft pseudopotentials to the projector augmented-wave method. Phys. Rev. B 59, 1758.

Lin, J.F., Speziale, S., Mao, Z., Marquardt, H., 2013. Effects of the electronic spin transitions of iron in lower mantle minerals: Implications for deep mantle geophysics and geochemistry. Rev. Geophys. 51, 244–275.

Lin, J.F., Struzhkin, V.V., Jacobsen, S., Hu, M.Y., Chow, P., Kung, J., Liu, H., Mao, H.K., Hemley, R.J., 2005. Spin transition of iron in magnesiowustite in the Earth's lower mantle. Nature 436, 377–380.

Mao, H.K., Shen, G., Hemley, R.J., 1997. Multivariable dependence of Fe–Mg partitioning in the lower mantle. Science 278, 2098–2100.

Mao, W.L., Mao, H.K., Sturhahn, W., Zhao, J.Y., Prakapenka, V.B., Meng, Y., Shu, J.F., Fei, Y.W., Hemley, R.J., 2006. Iron-rich post-perovskite and the origin of ultralow-velocity zones. Science 312, 564–565.

Martinez, I., Wang, Y., Guyot, F., Liebermann, R.C., Doukhan, J., 1997. Microstructures and iron partitioning in (Mg, Fe)SiO_3 perovskite-(Mg, Fe)O magnesiowustite assemblages: an analytical transmission electron microscopy study. J. Geophys. Res. 102, 5265–5280.

McCammon, C.A., Lauterbach, S., Seifert, F., Langenhorst, F., van Aken, P.A., 2004. Iron oxidation state in lower mantle mineral assemblages – I. Empirical relations derived from high-pressure experiments. Earth Planet. Sci. Lett. 222, 435–449.

Metsue, A., Tsuchiya, T., 2012. Thermodynamic properties of (Mg, Fe^{2+})SiO_3 perovskite at the lower-mantle pressures and temperatures: an internally consistent LSDA+U study. Geophys. J. Int. 190, 310–322.

Muir, J.M.R., Brodholt, J., 2015a. Elastic properties of ferropericlase at lower mantle conditions and its relevance to ULVZs. Earth Planet. Sci. Lett. 417, 40–48.

Muir, J.M.R., Brodholt, J., 2015b. Elastic properties of ferrous bearing $MgSiO_3$ and their relevance to ULVZs. Geophys. J. Int. 201, 496–504.

Nakajima, Y., Frost, D.J., Rubie, D.C., 2012. Ferrous iron partitioning between magnesium silicate perovskite and ferropericlase and the composition of perovskite in the Earth's lower mantle. J. Geophys. Res. 117, B082011–B082012.

Narygina, O., Dubrovinsky, L., Samuel, H., McCammon, C., Kantor, I., Glazyrin, I., Pascarelli, S., Aquilanti, G., Prakapenka, V., 2011. Chemically homogeneous spin transition zone in Earth's lower mantle. Phys. Earth Planet. Inter. 185, 107–111.

Nose, S., 1984. A molecular-dynamics method for simulations in the canonical ensemble. Mol. Phys. 52, 255–268.

Ono, S., 2008. Experimental constraints on the temperature profile in the lower mantle. Phys. Earth Planet. Inter. 170, 267–273.

Perdew, J.P., Ruzsinszky, A., Csonka, G.I., Vydrov, O.A., Scuseria, G.E., Constantin, L.A., Zhou, X.L., Burke, K., 2008. Restoring the density-gradient expansion for exchange in solids and surfaces. Phys. Rev. Lett. 100, 1364061–1364064.

Persson, K., Bengtson, A., Ceder, G., Morgan, D., 2006. Ab-initio study of the composition dependence of the pressure-induced spin transition in the (Mg_{1-x}, Fe_x)O system. Geophys. Res. Lett. 33, L163061–L163065.

Prescher, C., Langenhorst, F., Dubrovinsky, L., Prakapenka, V., Miyajima, N., 2014. The effect of Fe spin crossovers on its partitioning behavior and oxidation state in a pyrolitic Earth's lower mantle system. Earth Planet. Sci. Lett. 399, 86–91.

Sakai, T., Ohtani, E., Terasaki, H., Sawada, N., Kobayashi, Y., Miyahara, M., Nishijima, M., Hirao, N., Ohishi, Y., Kikegawa, T., 2009. Fe–Mg partitioning between perovskite and ferropericlase in the lower mantle. Am. Mineral. 94, 921–925.

Scanavino, I., Belousov, R., Prencipe, M., 2012. Ab initio quantum-mechanical study of the effects of the inclusion of iron on thermoelastic and thermodynamic properties of periclase (MgO). Phys. Chem. Miner. 39, 649–663.

Sinmyo, R., Hirose, K., 2013. Iron partitioning in pyrolitic lower mantle. Phys. Chem. Miner. 40, 107–113.

Sinmyo, R., Hirose, K., Nishio-Hamane, D., Seto, Y., Fujino, K., Sata, N., Ohishi, Y., 2008. Partitioning of iron between perovskite/postperovskite and ferropericlase in the lower mantle. J. Geophys. Res. Solid Earth 113, B112041-11.

Tange, Y., Takahashi, E., Nishihara, Y., Funakoshi, K.-i., Sata, N., 2009. Phase relations in the system MgO–FeO–SiO_2 to 50 GPa and 2000 °C: an application of experimental techniques using multianvil apparatus with sintered diamond anvils. J. Geophys. Res. Solid Earth 114.

Vilella, K., Shim, S.H., Farnetani, C.G., Badro, J., 2015. Spin state transition and partitioning of iron: effects on mantle dynamics. Earth Planet. Sci. Lett. 417, 57–66.

Walas, S., 1985. Phase Equilibria in Chemical Engineering. Butterworth Publ.

Wentzcovitch, R., Justo, J.F., Wu, Z., da Silva, C.R.S., Yuen, D., Kohlstedt, D., 2009. Anomalous compressibility of ferropericlase throughout the iron spin cross-over. Proc. Natl. Acad. Sci. 106, 8447–8452.

Wicks, J.K., Jackson, A., Sturhahn, W., 2010. Very low sound velocities in iron-rich (Mg, Fe)O: implications for the core-mantle boundary region. Geophys. Res. Lett. 37, L153041–L153045.

Wu, Z., Justo, J.F., da Silva, C.R.S., de Gironcoli, S., Wentzcovitch, R., 2009. Anomalous thermodynamic properties in ferropericlase throughout its spin crossover. Phys. Rev. B 80, 0144091–0144098.